EVLA Memo 113

Beam Squint and Stokes V on the VLA

W. D. Cotton and Juan M. Uson
NRAO [1]

Abstract

Radio telescopes with off–axis feeds such as the (E)VLA suffer from "Beam Squint" in which the two orthogonal polarizations sampled have different pointing centers on the sky. The effect of this is small near the beam center but is increasingly important towards the edge of the antenna power pattern where there are significantly different gains in the two polarizations. This effect has seriously limited the usability of the VLA for measuring circular polarization (Stokes V) and introduces dynamic range limiting wide–field artifacts in Stokes I. An adaptation of the visibility–based CLEAN [5] can correct for this effect. Examples are given of this technique being applied using the Obit (http://www.cv.nrao.edu/∼bcotton/Obit.html) package which allows wide–field imaging in Stokes V and reduced artifacts in Stokes I. This technique can be generalized to deal with temporally and spatially variable corrections.
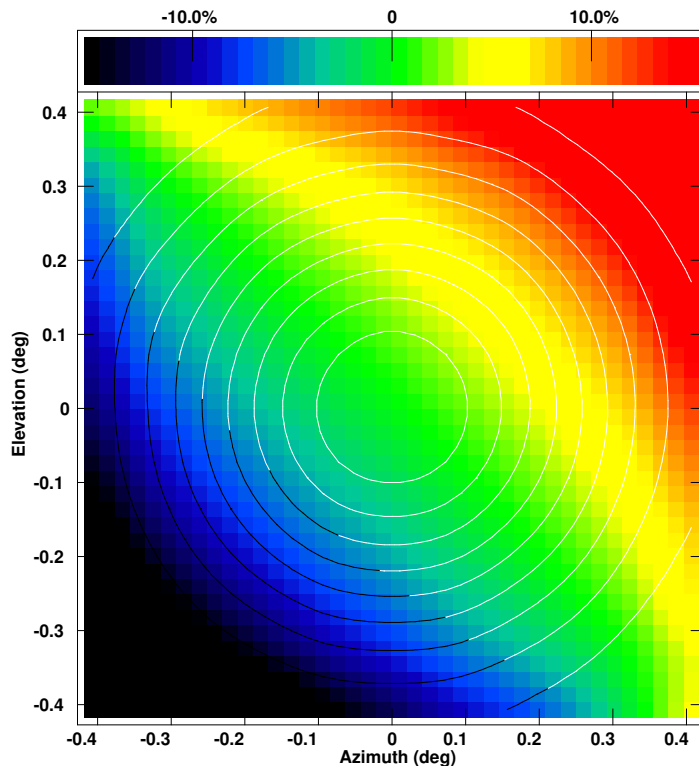
Contents

List of Figures

Figure 1: The VLA primary antenna pattern as measured during the NVSS survey [3] at 1.4 GHz. The instrumental Stokes V is shown in color with a scale bar at the top and contours are plotted every 10 percent in power.

1   Introduction

The enhanced sensitivity of the EVLA will allow it to study sources much weaker than are currently routinely observed. For frequencies at the lower end of the EVLA range this will generally require imaging the full primary beam of the antenna pattern, or at least the portions containing the stronger sources in the field in order to remove their side-lobes from the region of interest. In this regime, numerous effects of minor importance to observations of strong sources near the antenna pointing position must be understood and removed for the EVLA to reach its potential. "Beam Squint" resulting from the off–axis arrangement of the feeds is one of these effects. Beam squint has roughly equal and opposite effects on RR and LL measurements so images in Stokes I are only weakly affected by beam squint over most of the primary beam (as long as both visibilities for each polarization pair were observed and "survived" the editing stages at any given time stamp). The effect of the beam squint on the measured VLA beam at 1.4 GHz is shown in Figure 1 with the instrumental Stokes V (due to the beam squint) displayed in color and the total intensity in contours every 10 percent in power.

However, many galactic objects have significant circular polarization in their emission. Without correction for the beam squint, the (E)VLA has strong off–axis instrumental circular polarization [4] which masks any intrinsic circular polarization. Correction for the beam squint will allow much more sensitive studies of circular polarization.

(E)VLA observations are normally done in orthogonal polarizations (RCP and LCP). It has been known for quite some time that the antenna gain pattern formed on the sky for these two polarizations is not concentric, having a relative offset of 0.06 ± 0.005 of the antenna power FWHM; in reasonable agreement with a calculated value of 0.053 [8]. A subsequent, more refined model predicted a value of $28.6''$ at a frequency of 5 GHz [7]. Straightforward scaling with frequency leads

to a value of $1.70'$ at 1.4 GHz, in good agreement with the value measured by the NVSS team $(1.71' \pm 0.02')$ [3] corresponding to $0.055 \times$ FWHM. Thus, for perfectly pointed observations, the gain in RCP and LCP towards a source away from the pointing position will be modulated by up to $\sim 7\%$ in approximately opposite sense below or above the nominal gain depending on the relative orientation of the feed and source. The effect in RCP and LCP will be approximately equal in magnitude but of opposite sign and thus will largely cancel when estimating Stokes I; as long as both polarizations have been observed.

This report discusses the potential for correction of this effect and applies a correction method to observations made with the VLA. The possible extension of this technique to a wider class of time and/or direction-dependent corrections is discussed. All data manipulation discussed in this report use the Obit package (http://www.cv.nrao.edu/~bcotton/Obit.html) and plots were generated in AIPS.

2   Beam Squint Correction Technique

The beam squint can be characterized as a coupled offset in pointing of the two orthogonally polarized beams. The antenna will be nominally pointed using the midpoint of these two beams giving an effective pointing error in each beam. In the following, the beam squint is dealt with as a polarization dependent pointing error.

The beams are offset orthogonally to the line connecting the feed and the antenna center. Due to the alt-az mounts of the VLA antennas, this offset will rotate on the sky with parallactic angle. Note: by construction of the mounts, the VLA antennas all have the same parallactic angle even in the extended configurations.

The effect of beam squint on a given source depends on its location in the field of view, so in general, there is no operation on the uv data which removes the effect of beam squint over the whole field. The effects of beam squint can be included whenever the instrumental response to a model (e.g., a set of CLEAN components) is computed. In the algorithm described here, this is done using a discrete Fourier transform ("DFT" in AIPS-speak) where the instrumental response for each visibility is computed for each component and then summed over component. The flux density of the component is modified by the ratio of the antenna gain in the nominal pointing direction to the actual, beam squint dependent, gain. This is done independently for each polarization. As the beam squint rotates with parallactic angle, this flux density correction is time as well as direction dependent.

There are two cases where this interferometer response model is used. The first is in a visibility based ("Schwab-Cotton"[5]) CLEAN in which a set of components is initially located by a major cycle of the "Clark"[2] CLEAN followed by an accurate model calculation allowing the effects of those components to be removed from the visibility data and a new residual image derived from the residual visibility data. Thus, errors in the initial image due to inadequacies in the initial response model are corrected as deconvolution progresses.

The other use of the instrumental response model is in self–calibration in which the visibility data is divided by the instrumental response to the sky model to produce a dataset equivalent to observations of a point source. Using an accurate beam squint model allows removal of the effects of beam squint from the resultant gain solution.

If an image in Stokes V is desired, then Stokes I must be imaged first and the I model subtracted from the data applying beam squint corrections. This should remove the instrumental circular polarization from the data. Following this, the Stokes V image can be derived and deconvolved without further beam squint corrections. Instrumental leakage terms (the so-called D-terms) have been ignored in the procedure discussed in this note, but could be incorporated easily if necessary.

Table 1: VLA and EVLA Squint Azimuths

Band	VLA (nom.) °	VLA (modcomp) °	VLA (meas.) °	EVLA (nom.) °	EVLA (meas.) °
L	-135	-136.38	-136.8 ± 0.5	-84.1	——
S	—-	—-	—-	101.6	—-
C	65	61.33	60.1 ± 0.6	165.2	165.6 ± 1.7
X (6,14,22)	7	8.62	9.7 ± 0.5	-156.3	-156.3 ± 0.4
X (rest)	-50	——	-48.6 ± 0.3	as above	as above
Ku (11 ant)	115	120.2	113.5 ± 0.7	47.6	——
Ku (16 ant)	115	120.2	127.8 ± 0.5	as above	——
K (6, 14, 22)	96	89.13	91.1 ± 2.1	25.9	——
K (8 ant)	-16	——	-4.5 ± 1.1	as above	——
K (16 ant)	-16	——	-25.4 ± 1.2	as above	——
Q (6, 14, 22)	-21	-19.5	-20.8 ± 1.9	4.5	——
Q (rest)	5	——	6.0 ± 0.7	as above	——

2.1 CLEAN Model for Beam Squint Corrections

In the normal DFT model calculation, a list of CLEAN components is kept, and for each visibility measurement, the instrumental response to that component is calculated and the total instrumental response is the sum over all components. To apply the beam squint correction, the time- and polarization-dependent antenna gain corrections are used to adjust the component flux density for the effects of beam squint on the antenna power pattern. To do this, the antenna voltage gain relative to the nominal pointing is determined for the RCP and LCP beams in the direction of each CLEAN component and the interferometer power gain correction is the product of the antenna voltage gain corrections. The component gains are updated whenever the observing parallactic angle changes by as much a one degree. Again, this interval could be shortened if necessary.

A mixed array such as the VLA+EVLA adds another complication as the feed placement is different for the two types of antennas. For the VLA+EVLA, the right– and left–hand voltage gains are computed separately for VLA and EVLA antennas and the appropriate voltage gains are applied to the component flux density for each baseline. This is the implementation described in the following. The VLA is actually a mixed-array at some bands as the feed placement is not uniform. Antennas 6, 14 and 22 on the VLA have their X and K band (and subsequently their Q-band) feeds located at a different position than the remaining VLA antennas, see the Table below ([9]).

The implementation above assumes that all antennas have the same parallactic angle. For arrays such as the VLBA, parallactic angle will differ from antenna to antenna and an implementation for such an array would need to keep lists of voltage gain corrections for each antenna.

If large numbers of CLEAN components are involved, this technique is expensive in computer cycles and memory. A simple expedient procedure is to "compress" the list by summing the flux density of all components derived from a given image grid cell and using at most one component per cell. This is used in the Obit implementation.

2.2 Beam Squint Gain Corrections

An implementation of this beam squint correcting algorithm was made in the Obit package. The pointing offset in antenna coordinates due to the beam squint is computed according to the expression given by Napier [7] orthogonally to the line from the feed to the antenna center. Thus, the

offset for each polarization for the VLA is given by

$$\text{squint} \;=\; 237.56 \times \lambda \left(\frac{arcsecond}{meter} \right) \qquad \text{eq. 1)}$$

where λ is the wavelength (m). The value of squint is negative for LCP and positive for RCP. The offsets in RA and Dec are then:

$$\text{dx} = \text{squint} * (-sin(\text{feedAngle} - \chi)) \qquad \text{eq. 2a)}$$

$$\text{dy} = \text{squint} * (cos(\text{feedAngle} - \chi)) \qquad \text{eq. 2b)}$$

where feedAngle is the orientation of the feed on the feed circle, χ is the parallactic angle and the sign of squint is appropriate for the polarization. The locations of the various feeds for the VLA and EVLA are given in Table 1.

For a given CLEAN component, the distance from the pointing position corrected for beam squint is given by:

$$d(dx, dy) \;=\; arccos\{sin(\delta_{off})sin(\delta_{Pnt}) \;+\; cos(\delta_{off})\, cos(\delta_{Pnt})cos(\alpha_{off} - \alpha_{Pnt})\} \qquad \text{eq. 3)}$$

where α_{Pnt} and δ_{Pnt} are the RA and Dec of the antenna pointing, $\alpha_{off} \;=\; \alpha_{CC} + \text{dx}$, $\delta_{off} \;=\; \delta_{CC} + \text{dy}$, and α_{CC} and δ_{CC} are the RA and Dec of the component

For frequencies above 1 GHz, the antenna pattern is approximated above the 5% level by a Jinc function which is in turn approximated using [1]:

$$P(dx, dy) \;=\; 4.0\{0.5 + u(c1 + u(c2 + u(c3 + u(c4 + u(c5 + u\ c6)))))\}^2 \qquad \text{eq. 4)}$$

where

$$u \;=\; \{4.487e - 9 \times \left(\frac{25.0}{d_{ant}} \right) \times d(dx, dx) \times \nu\}^2 \; / \; 9.0$$

and c1=-0.56249985, c2=0.2109357,c3=-0.0395428, c4=0.00443319, c5=-0.00031761, c6=0.0000110 and d_{ant} is the antenna diameter in meters. Given the tapered illumination of the VLA primary reflector, at 1.4 GHz the beam is best fit with $d_{ant} \sim 24.5$ meter [3]. The voltage gain for each antenna and polarization is then:

$$\text{voltage\_gain} \;=\; \sqrt{\frac{P(0,0)}{P(dx, dy)}}$$

As described above, the correction assumes a single azimuthally–symmetric antenna pattern describable by a 1–D function. A single 2-D antenna pattern would be a simple modification. Antenna–specific antenna patterns require maintaining separate lists of component gains for each antenna.

In the case of a large number of components, this method can be time consuming. However, if the purpose of the application of this technique is solely to improve the dynamic range in Stokes I by reducing the artifacts arising from the brightest emission in the field; it is not necessary to compute a high accuracy model for components corresponding to regions of weaker emission. By restricting the accurate model calculation to the portion of the model representing the brightest emission and allowing faster, but less accurate calculations for the weaker emission, the expense of this algorithm can be drastically reduced. If Stokes V imaging is desired, the beam squint correction must be applied to the entire Stokes I model. In the implementation described here, a threshold is defined specifying the cutoff between the level needing the high accuracy model and that not. During CLEANing, whenever the peak in the initial residual image at the start of a major cycle exceeds this value, the high accuracy model is required for all components. When the peak residual drops below this value, a lower accuracy model calculation is allowed if it is

deemed to be faster. For self calibration or other cases where the total CLEAN model is known, the components corresponding to a given image cell are combined and those with flux densities exceeding the threshold use the high accuracy models and those below the threshold may use a faster method. In all cases, components corresponding to a given cell are combined before the model calculation. This might limit the dynamic range because of its effect on the amplitude self-calibration; a lower threshold leads to higher accuracy if it is needed, although at the expense of execution time. An extension of this procedure that would apply these criteria to the integrated fluxes rather than the peak values is being considered.

In Obit, this technique is implemented in the UV imager class ObitUVImageSquint, Sky Model ObitSkyModelVMSquint and in the task Squint.

2.3   Correction of Individual Antenna Patterns

Detailed differences among antennas will cause differences in their radiation patterns. For extremely high dynamic range, wide–field observations, corrections for these differences amoung antennas will be necessary. This case is similar to the beam squint problem in that time and direction gain corrections are needed. The technique described here for beam squint knows which antennas and polarizations are involved and a straightforward modification would allow correcting for detailed antenna patterns.

2.4   Antenna Pointing Errors

As mentioned in the introduction, in the absence of pointing errors, the effects of beam squint on RR and LL correlations will be approximately equal but of opposite sign. Thus, in this case, imaging of Stokes I (0.5 *(RR+LL)) will be largely, but not completely, insensitive to beam squint. However, if the pointing errors are not zero, the magnitude of beam squint on RR and LL will be different and will not be eliminated by imaging Stokes I, or by the technique described here without additional pointing corrections.

2.5   Correction of Pointing Errors

If post–observation corrections of antenna pointing errors are ever desired, a modification of this technique could be applied. Effective component gains for each antenna and polarization could be kept which include the antenna pointing errors as well as the beam squint. A time and antenna dependent addition to the beam squint position offsets would be used in computing the effective component gains.

3   Verification Using Test Data

The beam squint algorithm was tested on VLA B configuration observations of 3C84 alternating among having the source on-axis, at the 1/2 power of the antenna pattern west and 1/2 and 1/3 powers of the beam south of the pointing. Observations were made both in L and C band in spectral line mode, recording 15 × 390 kHz channels. The observations were made in July and August 2006. EVLA antennas were eliminated from the analysis because of the different location of the feeds as the procedure had not yet been extended to allow processing of data from a mixed array. The data were amplitude, phase and bandpass calibrated in the normal fashion

A convenient way to see the effects of beam squint and to test the efficacy of the correction is to examine a plot of the time-averaged Stokes V amplitudes averaged over baseline and spectral channel. The instrumental polarization is fixed to the antenna and will rotate with parallactic angle causing a time variable Stokes V signal in the averaged data. Since the relevant data did not have the source at the phase center, this averaging must be amp–scalar and therefore suffer a
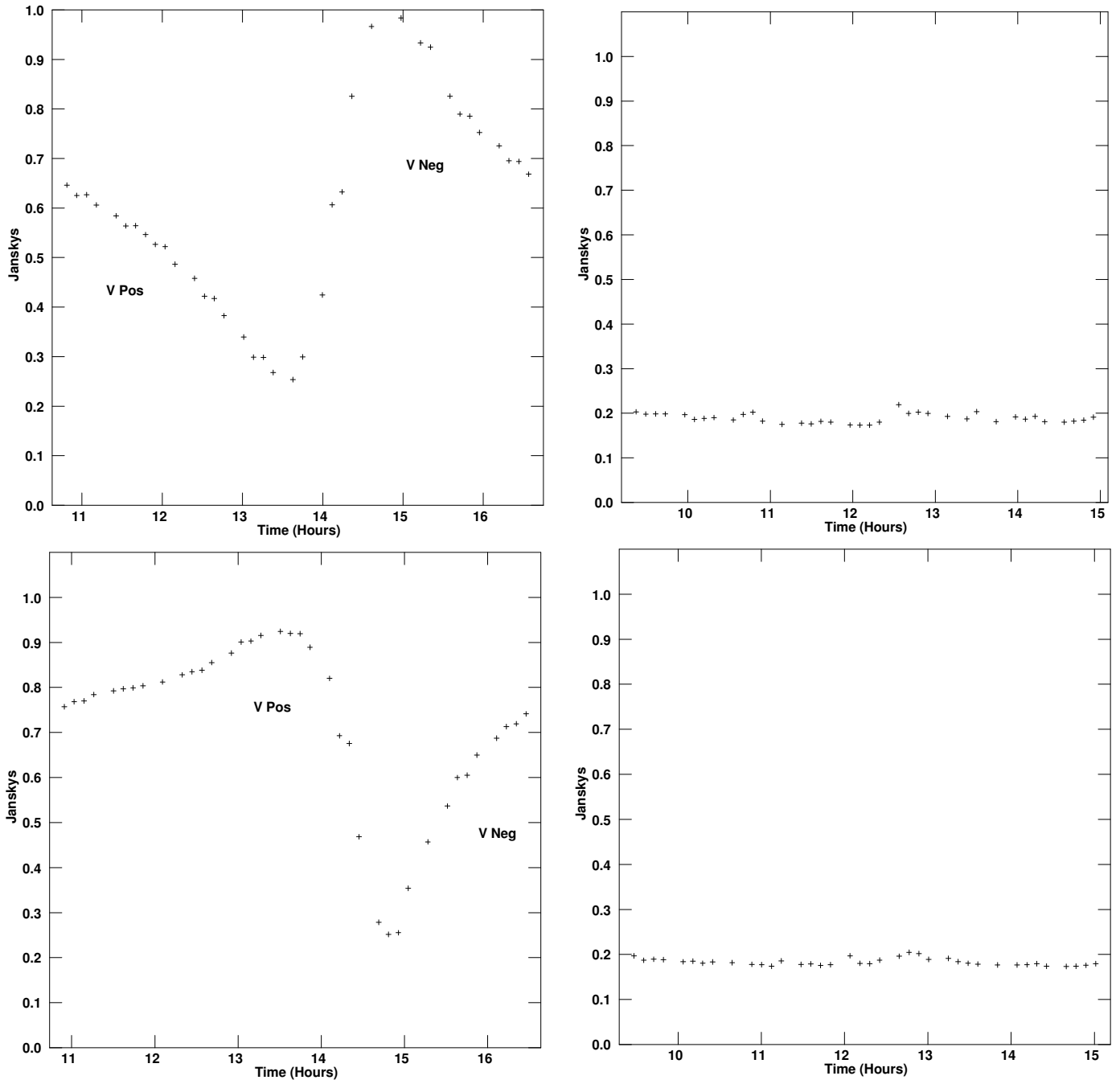
Figure 2: **Top:** Time averaged L band Stokes V for observations with 3C84 at the half power point west of the pointing center. On the left is the uncorrected data, the minimum is where the Stokes V changes sign; positive and negative regions of Stokes V are indicted. On the right, data after the subtraction of the beam squint corrected Stokes I model. The amplitude bias of the individual measurements is 200 mJy.
Bottom: As above, but with 3C84 at the 1/3 power of the antenna pattern south of the pointing center
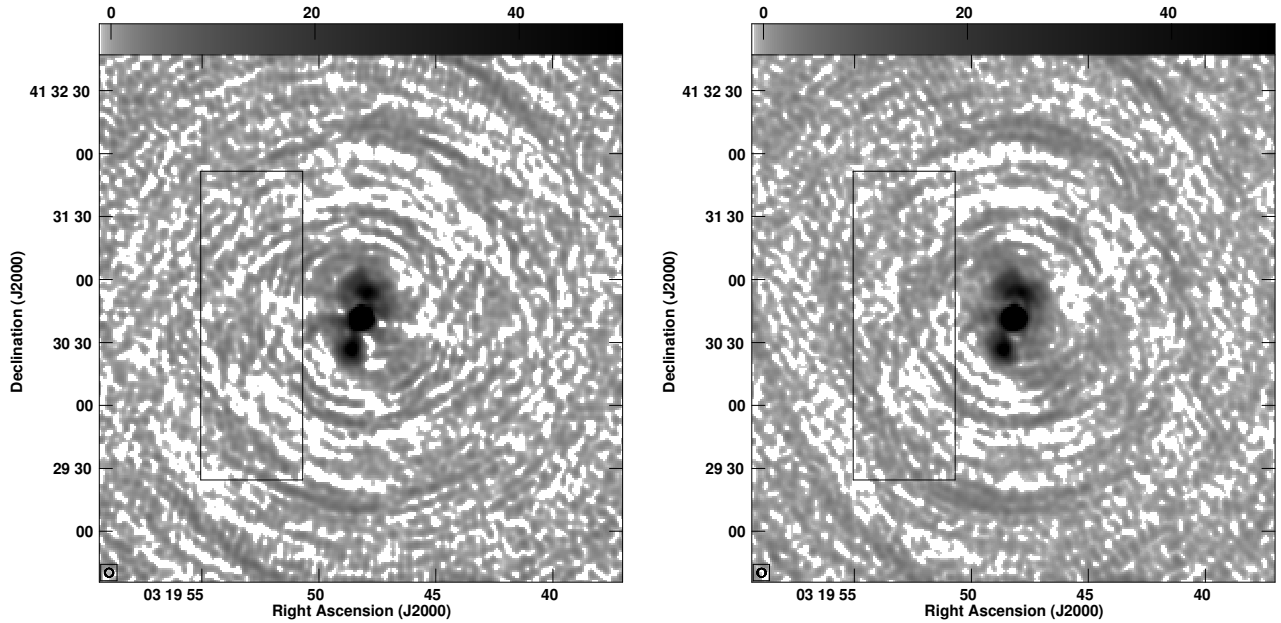
Figure 3: **Left:** Example 1 Stokes I in reverse grayscale of the region around 3C84 imaged with no beam squint correction. The image is displayed with a square root transfer function and the scale is given by the wedge (in mJy) at the top. The box gives the region over which the RMS was determined.
Right: As left but with beam squint corrections.

significant amplitude bias. Also, since the amplitude is shown, both positive and negative Stokes V are shown as positive with a dip in the curve where thre instrumental response goes from one to another. Several such plots are shown in Figure 2.

To test the beam squint correction algorithm, each data set was imaged using the beam squint corrections to derive a Stokes I model which was then subtracted, with squint corrections, from the data. A time averaged Stokes V plot, as shown in Figure 2, will show if the procedure has worked. The 200 mJy level in Figure 2 corresponds to the amplitude bias of the individual time and spectral samples. This figure shows that, to the accuracy of the display, the beam squint has been corrected. Similar results were obtained for the C band data.

4 Imaging Example 1

The first imaging example is of the 3C84 data at the half power point of the antenna pattern shown in the previous section. The data were processed twice, once without and once with beam squint corrections but otherwise processing was the same. All imaging used the autoCenter technique ([6]) to enhance the dynamic range. After applying basic amplitude, phase and bandpass calibration, the data were subjected to a single iteration of phase only self–calibration with a solution interval of 30 seconds. This was followed by a single iteration of amplitude and phase self–calibration with a 2 min. solution interval. Self–calibration solutions were determined for an average of right– and left–hand circular polarization as without beam squint corrections, the independent right– and left–hand amplitude self calibration would "correct" the data for 3C84 at the expense of the rest of the field.

The Stokes I images are shown in Figure 3 with a square-root stretch of the lower pixel values in the image (peak 12.2 Jy). The image without beam squint corrections has visibly more residual artifacts than the image with corrections. To compare the two images qualitatively, an RMS was computed in identical boxes which are shown in Figure 3. The RMS in the image without correction
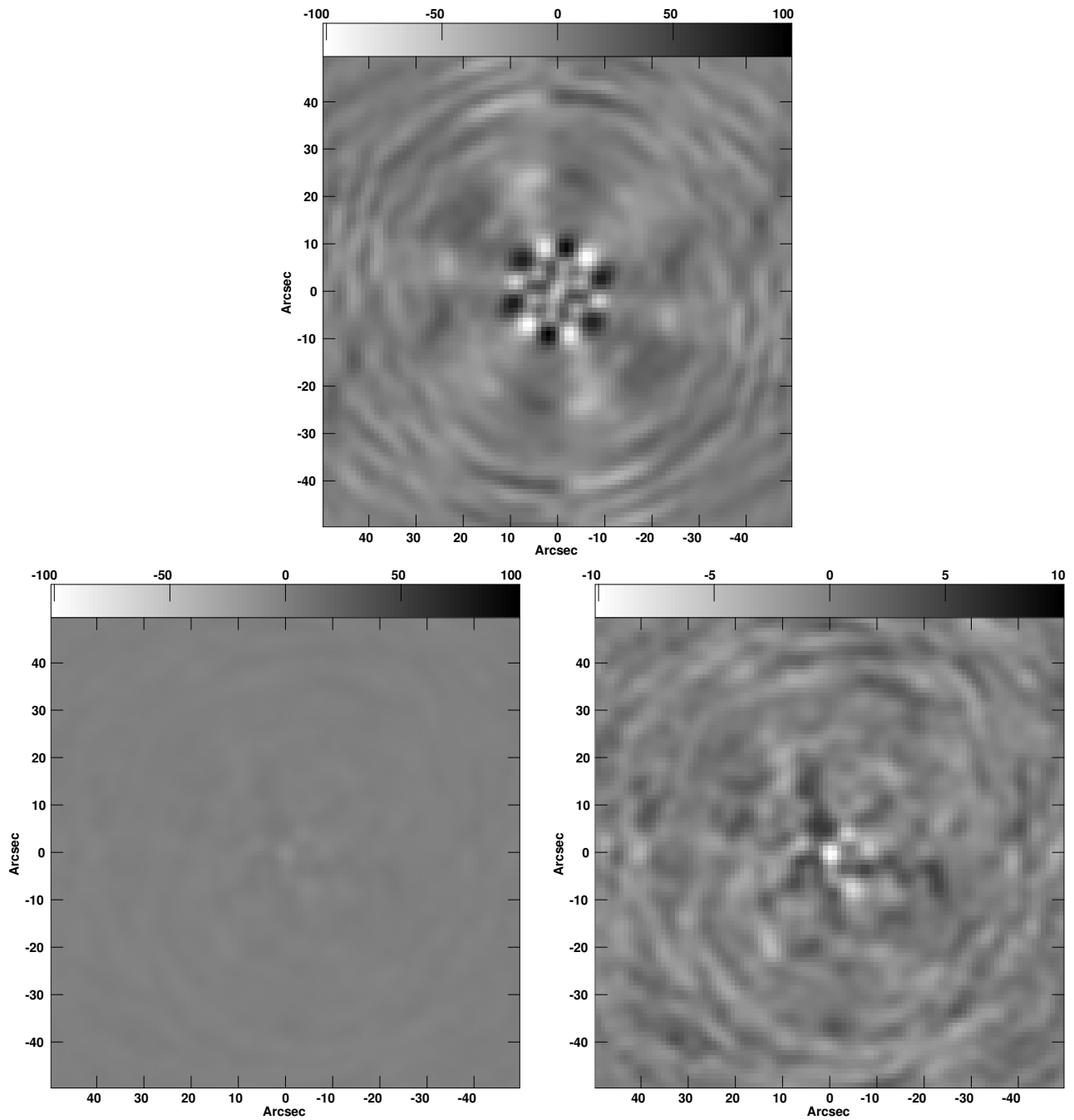
9

Figure 4: **Top:** Example 1 Stokes V in reverse grayscale of the region around 3C84 imaged with no beam squint correction shown with a linear display of -100 to 100 mJy/beam. The scale is given by the wedge at the top.
Bottom Left: As above but with beam squint corrections.
Bottom Right: As left but displaying the range of values -10 to 10 mJy/beam.
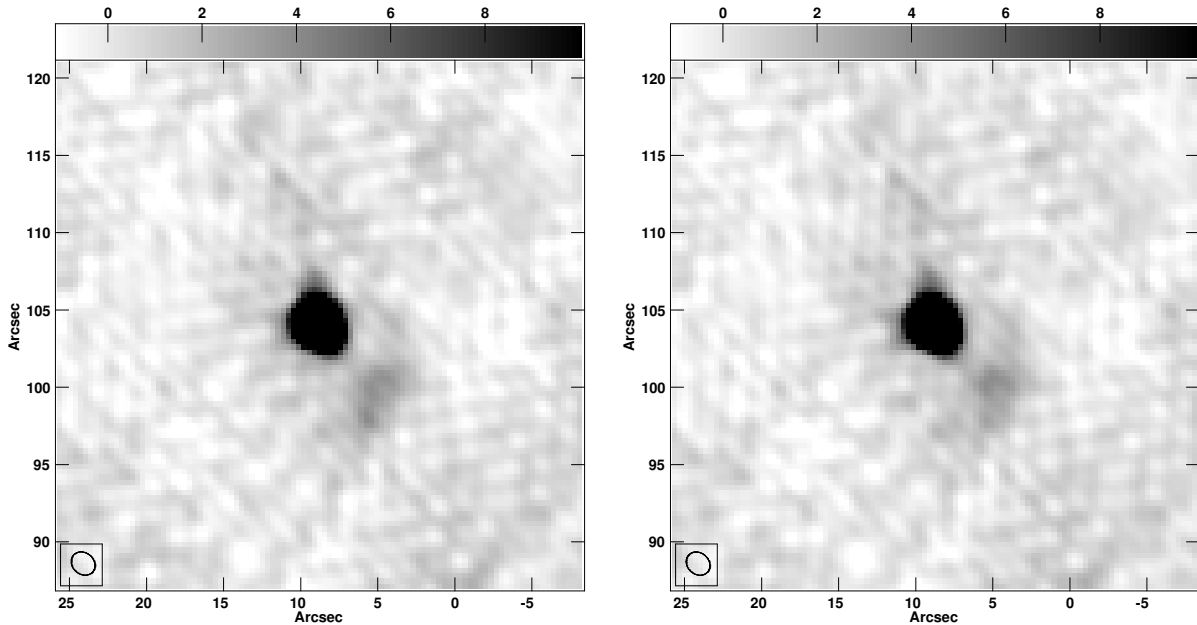
Figure 5: **Left:** Example 2 Stokes I in reverse grayscale of the region around source imaged with no beam squint correction. The image is displayed with the scale is given by the wedge (mJy) at the top.
Right: As left but with beam squint corrections.

was 1.39 mJy/beam and with corrections was 1.10 mJy/beam, or a reduction of the level of artifacts by 21%.

Figure 4 compares the Stokes V results. Since the data included observations over a range of parallactic angle, much of the instaneous instrumental circular polarization is washed out. The upper– and bottom–left frames show the same range of pixel values but in the latter (beam squint corrected) image little can be seen. The bottom right display gives the inner 10% of the pixel range in the bottom–left image. In the uncorrected image, the maximum and minimum values are well off the source but the maximum value in the corrected image is on–source. This analysis becomes confused as the core in this source is known to have circular polarization above the level shown in Figure 4. Since the data were calibrated using 3C84 and assuming no circular polarization, the polarization calibration is incorrect. Unfortunately no other calibrators were included in the observations.

In this test, the beam squint correction makes a significant improvement in the quality of the image in Stokes I and a very large improvement in the Stokes V image.

5   Imaging Example 2

The second example is a snapshot observation with the VLA in B configuration at C band. These data were taken in spectral mode with 2 IFs of 7 channels of 3.125 MHz in RR and LL and consists of approximately one minute of data. The usual calibration was applied to the data after which it was imaged with and without beam squint corrections. A single pass of phase self–calibration was followed by a single amplitude and phase self–calibration. Self–calibration averaged the RR and LL data before determining the solution. The results are shown in Figures 5 and 6. In this case, the Stokes I images are comparable with a peak of 279 mJy/beam, 364 mJy total CLEAN flux density, and an RMS off–source noise of 0.65 mJy/beam. The RMS values in the Stokes V images in Figure 6 are both 0.5 mJy/beam, but, whereas the beam squint corrected image shows no signal
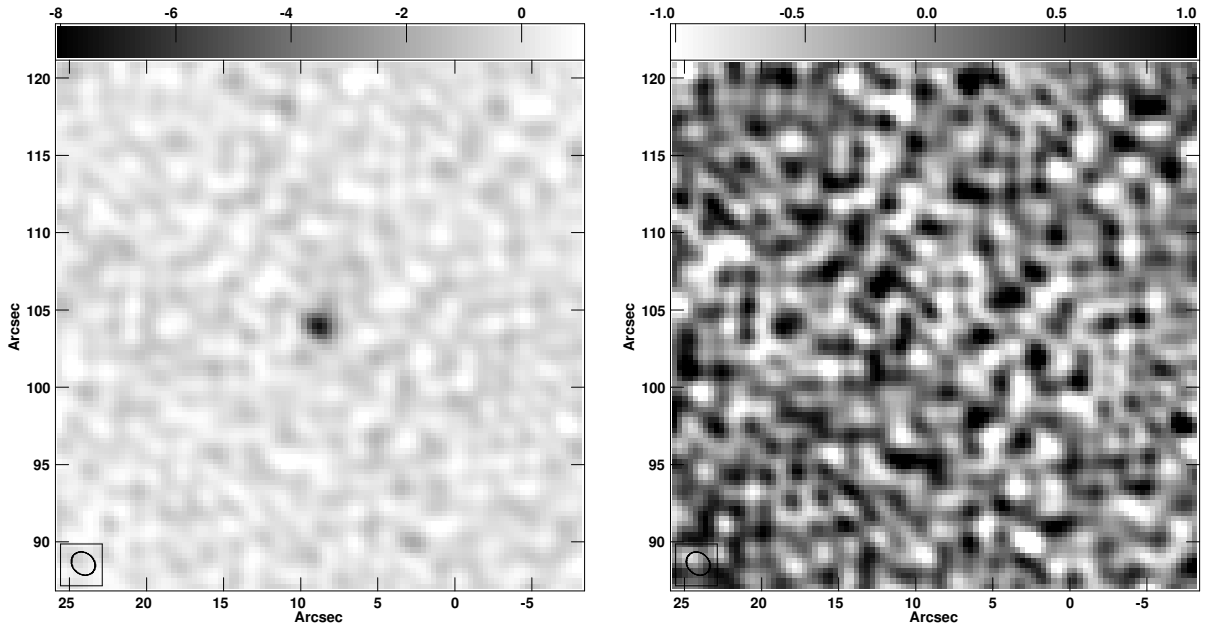
11

Figure 6: **Left:** Example 2 Stokes V in grayscale of the region around source imaged with no beam squint correction The scale is given by the wedge (mJy) at the top.
Bottom Left: As above but with beam squint corrections. Note different scale.

above the noise, the uncorrected image has a peak of -7.4 mJy/beam at the location of the Stokes I peak. This amounts to 2.7% instrumental circular polarization on a source relatively close to the pointing center. The one sigma upper limit for the corrected Stokes V image is 0.2%.

6   Conclusions

Taking advantage of the EVLA's increased sensitivity at lower frequencies (Ku band and below). will generally require imaging and deconvolving the entire primary beam, or at least the portions containing sources. Beam squint can produce artifacts well above the noise level.

This memo describes a technique for correcting VLA and EVLA observations for the effects of beam squint. The technique is a modification of the visibility based CLEAN in which the Stokes I image is made in the usual way, but when the image model is subtracted from the data, corrections are made such that the model includes the effects of beam squint. Thus, any errors made in the initial imaging are corrected through iterative imaging and accurate model subtraction.

Several tests of an implementation of this technique in the Obit task Squint were made. In all cases, careful calibration is critical. Observations of the strong source 3C84 were made with the source at various locations in the antenna pattern resulting in strong instrumental circular polarization. Both L and C band test data sets were processed. The implementation in task Squint corrects the beam squint induced instrumental circular polarization to a high degree.

Detailed examples of imaging one of the 3C84 L band data sets with the source at the half power point of the antenna pattern were given. Applying beam squint corrections improved the near in residual artifacts by more than 20% and very substantial improvements were made to the Stokes V image.

A second test of snapshot imaging of a weaker source at C band demonstrates the feasibility of searches for sources of circularly polarized emission. Uncorrected, the source had 2.8% instrumental circular polarization whereas, corrected, the one–sigma upper limit was 0.2%.

Extensions of this technique are possible to correct for individual antenna patterns and antenna

pointing errors. We find that we can obtain somewhat better results for the test observations discussed in this memo if we modify the nominal squint parameters by not–so–small amounts (up to a few degrees in position angle and up to a few percent in offset from the values indicated in Table 1 and Eqn. 1. We are investigating the pointing parameters of the (E)VLA antennas and hope to achieve a more accurate characterization of the squint parameters. We shall report on those results in due course.

References

[1] M. Abramowitz and I. A. Stegun. *Handbook of Mathematical Functions*. Washington, [National Bureau of Standards], 1964.

[2] B. G. Clark. An efficient implementation of the algorithm 'CLEAN'. *A&A*, 89:377–378, 1980.

[3] J. J. Condon, W. D. Cotton, E. W. Greisen, Q. F. Yin, R. A. Perley, G. B. Taylor, and J. J. Broderick. The NRAO VLA Sky Survey. *Astron. J.*, 115:1693–1716, May 1998.

[4] W. D. Cotton. Widefield Polarization Correction of VLA Snapshot Images at 1.4 GHz. *AIPS Memo Series.*, 86:1–9, 1994.

[5] W. D. Cotton. Special Problems in Imaging. In G. B. Taylor, C. L. Carilli, and R. A. Perley, editors, *Synthesis Imaging in Radio Astronomy II*, volume 180 of *Astronomical Society of the Pacific Conference Series*, pages 357–370, 1999.

[6] W. D. Cotton and J. M. Uson. Image Pixelization and Dynamic Range. *EVLA Memo 114*, ftp://ftp.cv.nrao.edu/NRAO-staff/bcotton/Obit/autoCen.pdf, 2007.

[7] P. J. Napier. Polarization Properties of an Open Cassegrain Antenna. *MMA Memo*, 115:1–17, 1994.

[8] P. J. Napier and J. J. Gustincic. "polarization properties of a cassegrain antenna with off-axis feeds and on-axis beam.". In *"Digest of the IEEE International Symposium"*, "Stanford: IEEE Antennas and Propagation Society", pages 452–454, 1977.

[9] J. M. Uson and W. D. Cotton. Everything you ever wanted to know about VLA Squint. *EVLA Memo Series.*, in preparation:1+, 2007.